Computational manufacturing as a key element in the design–production chain for modern multilayer coatings

Tatiana V. Amotchkina,[1,3,4,*] Sebastian Schlichting,[2] Henrik Ehlers,[2] Michael K. Trubetskov,[1,3] Alexander V. Tikhonravov,[1] and Detlev Ristau[2,4]

[1]Research Computing Center, Moscow State University, Leninskie Gory, Moscow 119991, Russia

[2]Laser Zentrum Hannover e.V., Hollerithallee 8, Hannover D-30419, Germany

[3]Max Planck Institute of Quantum Optics, Hans-Kopfermann-Straße 1, Garching D-85748, Germany

[4]QUEST—Centre for Quantum Engineering and Space-Time Research, Welfengarten 1, Hannover D-30167, Germany

*Corresponding author: tatiana@srcc.msu.ru

Received 5 July 2012; revised 1 October 2012; accepted 2 October 2012; posted 2 October 2012 (Doc. ID 171968); published 26 October 2012

We propose a general approach that allows one to reveal factors causing production errors in the course of the deposition process controlled by broadband optical monitoring. We consider computational experiments simulating the real deposition process as a crucial point of this approach. We demonstrate application of the approach using multiple experimental deposition runs of the selected multilayer coatings. © 2012 Optical Society of America

OCIS codes: 310.1860, 310.4165, 310.3840, 310.6860.

1. Introduction

In recent years demands on complex multilayer coatings with sophisticated performance specified in wide spectral ranges have been permanently growing [1,2]. Design and production of such coatings have become realistic due to tremendous progress in elaboration of stable deposition processes [3], high-precision monitoring techniques [1,4–7], advanced measurement instrumentation [8], and powerful design software tools [9]. Modern numerical algorithms allow one to design multilayer coatings with any desired spectral performance that does not contradict the fundamental laws of nature [2,10]. Accurate practical implementation of complex theoretical design solutions may, however, be a problem, even for advanced deposition plants equipped with precise monitoring devices, because of inevitable errors of different types. Evidently, in order to improve the reliability of production of complex designs, research efforts should be developed in two directions.

Research work for the first direction is to be aimed at elaborating adequate models of multilayer optical coatings, improving accuracy of existing monitoring algorithms, and developing novel monitoring strategies. Recent theoretical achievements already made in this direction, as well as corresponding experimental results, have been reported in [1,4,7,11–15]. Simulations of real deposition runs, so-called computational manufacturing experiments (CME), are used to test mathematical algorithms utilizing on-line monitoring data and controlling layer thicknesses [1,16,17].

Modern design approaches provide not one but a set of design solutions with excellent spectral performance and close combinations of principle design

1559-128X/12/317604-12$15.00/0

parameters (merit function value, number of layers, total optical thickness) [2,18]. Different design solutions, however, are not equally suitable for practical realization. For example, some of them may be unstable with respect to deposition errors and even cause failures of deposition processes [19]. On the other hand, other designs may exhibit stability to deposition errors, even to errors of large magnitudes. In general, stability of the design solutions is tightly interconnected with a monitoring technique used in the course of design deposition. The second direction of research efforts, therefore, is related to elaboration of numerical tools for selecting the most manufacturable designs among multiple solutions of considered design problems. At the current state of the art, CME, simulating real deposition runs, are intensively used for this purpose [1,12,16,19,20]. Recently, importance and benefits of CME have been demonstrated for the production of various types of optical coatings [7,12,20,21].

It is natural to define *the most manufacturable design* as a design providing the highest production yield. Evidently, performing a representative number of real deposition runs in order to find the production yield is quite expensive and time consuming. At the same time, expenses on CME are negligible in comparison with the costs of real experiments. CME provide an estimation of the production yield that is calculated as a ratio of the number of successful experiments to the total number of performed experiments [16,20,22,23]. To distinguish between successful and unsuccessful experiments, allowed corridors of deviations from target spectral characteristics are to be used. Experiments with spectral characteristics lying inside such corridors are considered as successful ones. Simulation algorithms allowing one to estimate the production yield are elaborated in several research groups [1,4,12,16,24].

It is reasonable, therefore, that computational manufacturing should be implemented in modern design-production chains of multilayer coatings as it is schematically shown in Fig. 1. The left-hand dashed rectangle in this figure illustrates the selection of the most manufacturable designs with the help of computational manufacturing.

Estimations of the production yield, however, can be considered as reliable ones only if in the course of

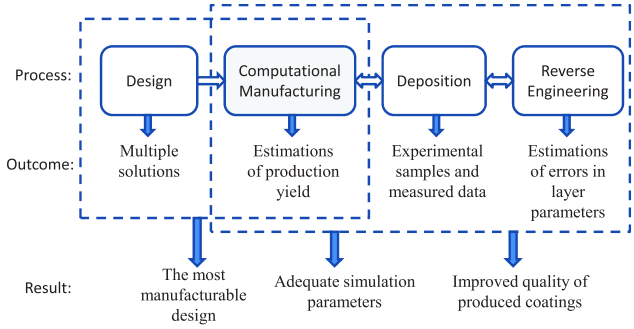

Fig. 1. (Color online) Schematic representation of modern design–production chain.

CME real deposition runs are adequately simulated. It means that most of the factors causing production errors in deposition plants must be taken into account by a simulator. It is important also that the numerical values of parameters representing these factors are of the same level as in the real deposition environment. One possible approach was proposed in [24], where a series of single-layer samples were produced in order to investigate the reproducibility of layer properties and specify deposition errors in the course of simulations.

The establishment of adequate relations between real and simulated deposition processes is not a straightforward research task. For this purpose an iterative procedure comprising CME, real deposition runs, and reverse engineering of produced coatings is required. The interconnection between simulation, deposition, and reverse engineering processes is also schematically shown in Fig. 1 (see right-hand dashed rectangle).

In the course of our present study we worked in the first research direction mentioned above. We performed multiple computational and real deposition experiments. On the basis of analysis of their results, we revealed main sources of deposition errors and found simulation parameters that adequately correspond to real deposition parameters. On the one hand, the obtained results helped us to provide feedback to deposition process and to produce coatings with improved spectral performance (right-hand dashed rectangle in Fig. 1). On the other hand, these results will allow us to work in the second research direction and raise the reliability of production yield estimations (left-hand dashed rectangle in Fig. 1). The latter will be discussed in our upcoming publication.

In the course of our research we produced a number of experimental samples using the ion-assisted deposition process based on the Leybold SYRUSpro1100 deposition plant equipped with an APSpro advanced plasma source. For monitoring of layer thicknesses, the broadband monitoring (BBM) system developed at the Laser Zentrum Hannover (LZH) was used. This BBM system provides fully automated process control based on *in situ* transmittance measurements on moving substrates [1,14,15,25].

We performed CME using two different software tools: the BBM simulator developed at the LZH [1,19,25] and a BBM simulator incorporated with OptiLayer thin film software [9].

In Section 2 we compare the results of our starting CME and the first series of real deposition runs and reveal that real deposition parameters and simulation parameters are not consistent. In Section 3 we recognize main factors causing deposition errors and find simulation parameters that adequately describe the deposition process. In Section 4 we validate our reverse engineering procedure using simulated and experimental data. In Section 5 we make corrections to the deposition process controlled

by BBM and produce coatings with improved spectral performance. Our main results are presented in the conclusions in Section 6.

Generally, in this paper we proposed an approach that allows researchers to establish relations between the simulation process, monitoring procedure, and reverse engineering process. This approach can also be used by researchers with not only BBM but any other optical monitoring technique at their disposal.

2. Starting Computational Manufacturing Experiments and First Deposition Runs

At the beginning of our study we considered two design problems: design of a narrow bandpass filter (NBPF) and design of a two-line filter (TLF). In the first design problem, the target transmittance $T^{(t)}(\lambda)$ is zero in the spectral ranges from 450 to 506 nm and from 545 to 650 nm and is 100% in the spectral range from 526 to 538 nm [26]. We designed two filters, denoted below as NBPF1 and NBPF2. These filters consist of 26 and 25 layers, respectively. Layer thicknesses of NBPF1 and NBPF2 designs are presented in Table 1. In the second design problem, the target transmittance is zero in the spectral ranges from 500 to 580 nm, from 615 to 693 nm, and from 720 to 800 nm and 100% in the ranges from 598 to 602 nm and from 698 to 702 nm [7]. For this problem, we found two design solutions, denoted as TLF1 and TLF2. Both designs contain 31 layers; design structures are shown in Table 1.

In the design process we used titanium dioxide as a high-index material and silicon dioxide as a low-index material. Refractive indices of these materials were specified by Sellmeier equations:

$$n^2(\lambda) = 1 + \frac{A_1\lambda^2}{\lambda^2 - A_2} + \frac{A_3\lambda^2}{\lambda^2 - A_4}, \quad (1)$$

where $A_1 = 4.017, A_2 = 0.0525, A_3 = 1.402, A_4 = 80$ for TiO_2 and $A_1 = 1.159, A_2 = 0.0015, A_3 = 0.5, A_4 = 61$ for SiO_2; λ in this formula should be expressed in micrometers. The extinction coefficient $k(\lambda)$ of TiO_2 was estimated as $k(400) = 0.0012$, $k(450) = 0.0005$, $k(500) = 0.0002$, $k(550) = 0.0001$, $k(600) = 0.0001$, $k(\lambda) = 0$ for $\lambda > 600$ nm. In what follows, we shall refer to these refractive indices and extinction coefficients as *nominal* ones. The substrate is Suprasil of 1 mm thickness; the refractive index is taken from the substrate manufacturer [27].

Evidently, in the case of chosen design problems, not only two but multiple solutions exist. We selected

Table 1. Structures of the Design Solutions

Layer Number	Physical Thickness (nm)				Layer Material
	NBPF1	NBPF2	TLF1	TLF2	
1	54.63	58.13	68.57	68.33	TiO_2
2	90.45	134.29	107.35	108.48	SiO_2
3	54.63	58.22	30.00	65.88	TiO_2
4	180.89	119.60	30.00	97.89	SiO_2
5	54.63	183.35	52.65	43.91	TiO_2
6	90.45	116.54	108.07	54.44	SiO_2
7	54.63	51.15	64.30	61.21	TiO_2
8	90.45	115.46	79.60	100.54	SiO_2
9	54.63	60.54	38.15	59.40	TiO_2
10	90.45	115.78	83.49	30.00	SiO_2
11	54.63	48.69	63.88	48.76	TiO_2
12	361.78	118.12	105.67	104.16	SiO_2
13	54.63	34.30	70.46	66.29	TiO_2
14	90.45	189.77	185.98	108.20	SiO_2
15	54.63	51.12	70.38	66.60	TiO_2
16	90.45	94.10	109.06	109.80	SiO_2
17	54.63	50.99	67.54	68.29	TiO_2
18	90.45	91.26	110.67	112.68	SiO_2
19	54.63	51.03	68.95	72.32	TiO_2
20	180.89	92.47	111.69	117.83	SiO_2
21	54.63	51.18	67.97	82.87	TiO_2
22	90.45	211.39	109.72	63.75	SiO_2
23	54.63	23.30	176.86	30.00	TiO_2
24	90.45	112.04	86.72	47.44	SiO_2
25	13.04	52.03	54.74	80.36	TiO_2
26	124.06		88.42	172.45	SiO_2
27			140.61	100.08	TiO_2
28			95.68	116.91	SiO_2
29			61.10	75.58	TiO_2
30			101.04	115.42	SiO_2
31			62.00	71.09	TiO_2

Table 2. Estimations of Production Yields Obtained in the Course of Starting CME

Design	BBM LZH Simulator			OptiLayer Simulator		
	Estimated Yield (%)	$\langle DF_{\text{sim}} \rangle$	$\langle DF_{\text{sim}}^{(t)} \rangle$	Estimated Yield (%)	$\langle DF_{\text{sim}} \rangle$	$\langle DF_{\text{sim}}^{(t)} \rangle$
NBPF1	100	3.3	0.3	100	1.3	0.5
NBPF2	100	3.9	0.7	100	2.3	0.7
TLF1	100	2.8	3.8	100	4.3	3.5
TLF2	0	—	—	15	3.0	4.2

only two solutions because we are only illustrating our approach and do not want to overload the study.

In order to analyze the stability of the selected designs to deposition errors and to estimate production yield of the chosen designs, we performed *starting* CME. In order to distinguish between successful and unsuccessful CME, we specified range targets. In the case of NBPFs, transmittance is to be less than 5% in the spectral ranges from 450 to 510 nm and from 552 to 650 nm and more than 90% in the spectral range from 528 to 536 nm. In the case of TLFs, transmittance is to be more than 90% at the wavelengths 600 and 700 nm.

In the course of starting CME, all major factors causing production errors in the real deposition chamber were simulated. The mean deposition rates for the low- and high-index materials were 0.56 nm/s and 0.3 nm/s, respectively; the root mean square (rms) fluctuations of SiO_2 and TiO_2 rates were specified as 12% and 3%, respectively. Mean shutter delays were taken equal to 350 ms; rms deviations of the shutter delay were taken equal 80 ms. Simulated BBM data were transmittance data measured in the spectral range from 420 to 950 nm; the time interval between measurements was 2 s. BBM transmittance data were simulated with random errors having approximately 1% noise level and 0.15% fluctuations of the whole transmittance curve. In the case of the BBM LZH simulator, the spectral distribution of the simulated noise reproduced the real noise of the spectrophotometer used by the BBM device. The wavelength resolution was also the same as in the spectrophotometer. Refractive index offsets for SiO_2 and TiO_2 were taken equal to 0.0035 and 0.001, respectively.

Estimations of production yields obtained in the course of starting CME are presented in the second and fifth columns of Table 2. Total number M of CME for each design was 50. We observed that the estimations of yield obtained by the two simulators are quite close. According to [20], with $M = 50$, the designs NBPF1, NBPF2, and TLF1 exhibit a production yield exceeding 88%; the design TLF2 exhibits a low production yield that is less than 11%. In Fig. 2 we show thickness errors made in the course of typical CME performed using the OptiLayer module and using the BBM LZH simulator. In Fig. 2 we observe that the two simulators give qualitatively similar levels of thickness errors.

In order to numerically estimate the closeness between theoretical transmittance $T(\lambda)$ and measured transmittance $\hat{T}(\lambda)$ of experimental or simulated coatings, we introduced a discrepancy function DF:

$$DF = \left(\frac{1}{L} \sum_{j=1}^{L} [T(\lambda_j) - \hat{T}(\lambda_j)]^2 \right)^{1/2}, \tag{2}$$

where $\{\lambda_j\}$ is the wavelength grid specified in the spectral range from 420 to 950 nm and L is the number of spectral points. We denote as DF_{sim} the value of the discrepancy function [Eq. (2)] calculated for the case when $\hat{T}(\lambda_j)$ is from the simulated measurement data. In the third and sixth columns of Table 2, we present average $\langle DF_{\text{sim}} \rangle$ values calculated on the basis of $M = 50$ starting CME as $(1/M) \sum_{i=1}^{M} DF_{\text{sim},i}$ [the number of spectral points $L = 1160$ in Eq. (2)].

From a practical point of view, it is useful to numerically estimate the closeness of the measured transmittance $\hat{T}(\lambda)$ of experimental or simulated coatings to the target transmittance $T^{(t)}(\lambda)$. In order to do this, we consider a *deviation* function $DF^{(t)}$:

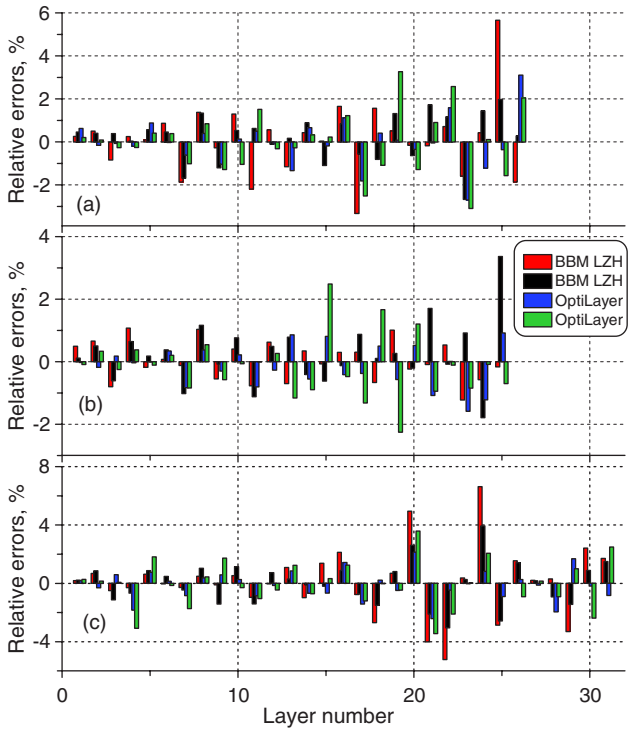

Fig. 2. (Color online) Typical relative errors in layer thicknesses made in the course of starting CME: (a) NBPF1, (b) NBPF2, (c) TLF1.

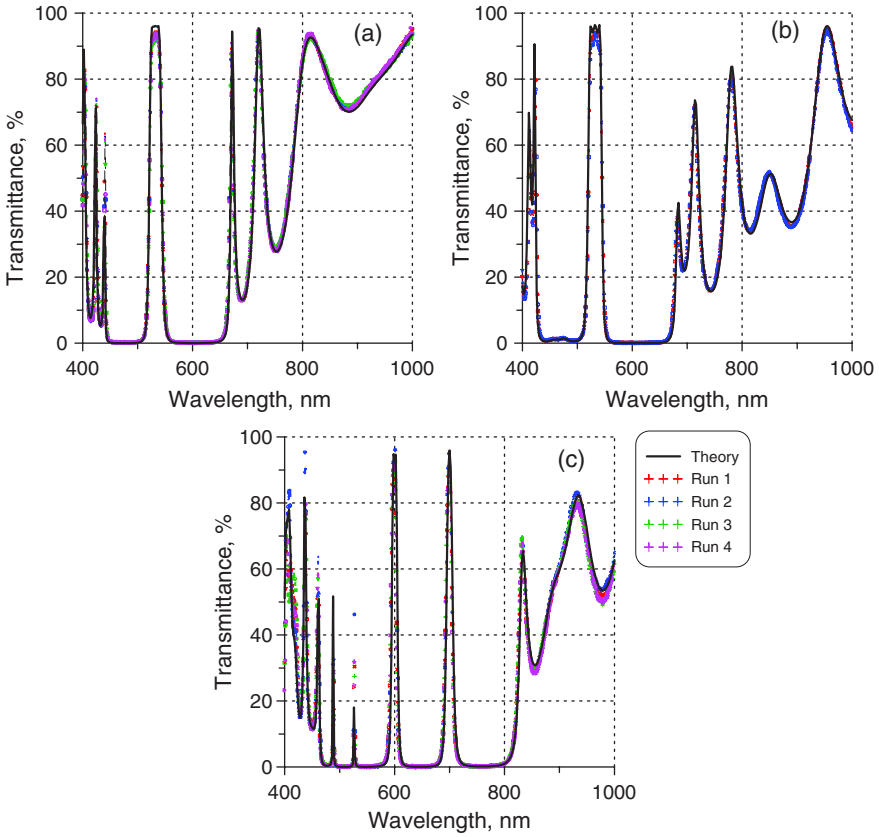

Fig. 3. (Color online) Theoretical transmittances of designs (a) NBPF1, (b) NBPF2, and (c) TLF1 (solid curves) and measured transmittance data of corresponding experimental samples (crosses).

$$DF^{(t)} = \left(\frac{1}{L}\sum_{j}[\hat{T}(\lambda_j) - T^{(t)}(\lambda_j)]^2\right)^{1/2}, \qquad (3)$$

where $\{\lambda_j\}$ is the uniform wavelength grid in the target spectral range. We denote as $DF^{(t)}_{\mathrm{sim}}$ the value of the deviation function [Eq. (3)] calculated for the case when $\hat{T}(\lambda_j)$ is from the simulated measurement data. Note that in the case of $DF^{(t)}$ [Eq. (3)] the wavelength grid λ_j and the number of wavelength points L are typically different from ones used for the definition of DF in Eq. (2). In the fourth and seventh columns of Table 2, we present average $\langle DF^{(t)}_{\mathrm{sim}}\rangle$ values calculated on the basis of M starting CME as $(1/M)\sum_{i=1}^{M} DF^{(t)}_{\mathrm{sim},i}$, $M = 50$. It is seen from Table 2 that the average $\langle DF_{\mathrm{sim}}\rangle$ and $\langle DF^{(t)}_{\mathrm{sim}}\rangle$ values, corresponding to two different simulators, are consistent.

We performed several real deposition runs for each design, namely, four runs for the NBPF1 design, two runs for the NBPF2 design, four runs for the TLF1, and three runs for TLF2. In the course of deposition of TLF2, all processes failed. It was expected because of the low estimation of production yield (see Table 2). All runs of designs NBPF1, NBPF2, and TLF1 were successful: deposition processes were finished properly, and spectral transmittance data of the produced samples were lying inside the allowed corridors. Spectral performance of the produced experimental samples are shown in Fig. 3. The transmittance curves corresponding to different runs are almost indistinguishable.

We denote DF_{exp} and $DF^{(t)}_{\mathrm{exp}}$ as the values of the discrepancy function [Eq. (2)] and deviation function [Eq. (3)] calculated for the case when $\hat{T}(\lambda_j)$ is from the experimental data. Values for DF_{exp} and $DF^{(t)}_{\mathrm{exp}}$ corresponding to the produced coatings are collected in Table 3.

Comparing DF_{sim} values (Table 2) and DF_{exp} values (Table 3), we observed that DF_{exp} values are essentially larger than DF_{sim} values. We noticed also that $DF^{(t)}_{\mathrm{exp}}$ values (Table 3) are larger than $DF^{(t)}$

Table 3. Discrepancies DF_{exp} and $DF^{(t)}_{\mathrm{exp}}$ Obtained for the First Deposition Runs

	NBPF1		NBPF2		TLF1	
Deposition Run\Design	DF_{exp}	$DF^{(t)}_{\mathrm{exp}}$	DF_{exp}	$DF^{(t)}_{\mathrm{exp}}$	DF_{exp}	$DF^{(t)}_{\mathrm{exp}}$
Run1	5.4	1.1	4.0	2.2	5.2	8.5
Run2	6.4	1.7	4.8	2.9	3.0	3.9
Run3	6.7	2.7			5.7	9.5
Run4	5.8	1.5			5.8	9.1

values (Table 2). This is an indication of the fact that the values of real deposition parameters and simulation parameters were not consistent. This may also mean that there were process disturbances that were not taken into account in the course of CME.

In order to compare real errors in layer thicknesses and errors obtained in the course of CME, we performed reverse engineering of the produced coatings. At our disposal we had transmittance data $\hat{T}^{(k)}(\lambda_j)$ recorded after the deposition of each layer $k = 1, \ldots, N$ by the BBM device and available on a set of wavelengths $\{\lambda_j\}$ in the spectral range from 420 to 950 nm, $j = 1, \ldots, L$, $L = 1196$. In our reverse engineering process we assumed that the optical constants of layers were known with sufficient accuracy and concentrated our attention only on errors in the thicknesses of the coating layers. We estimated relative errors $\delta_1, \ldots, \delta_N$ in layer thicknesses on the basis of minimization of the generalized discrepancy function [26,28]:

$$GDF = \left(\frac{1}{NL} \sum_{k=1}^{N} \sum_{j=1}^{L} [T^{(k)}(d_1(1+\delta_1), \ldots, d_k(1+\delta_k); \lambda_j) - \hat{T}^{(k)}(\lambda_j)]^2 \right)^{1/2}, \quad (4)$$

where N is the number of design layers, $T^{(k)}(\ldots)$ is the theoretical transmittance, corresponding to the part of the coating consisting of k layers, and $\hat{T}^{(k)}$ is the measured transmittance after the deposition of the layer number k.

The estimated relative errors in layer thicknesses are shown in Fig. 4. Analyzing Fig. 4, we observed a very interesting feature: the errors related to different experimental runs are quite close, i.e., the errors were reproduced from one deposition run to another. This tendency is observed for all three considered designs, even though the runs were performed in different deposition campaigns [see Figs. 4(a)–4(c)]. This suggests high reproducibility and a stable process. Dominating random influences can be excluded.

Comparing errors estimated from real experimental data (Fig. 4) and typical errors obtained in the course of CME (Fig. 2), we observed that the levels of estimated real errors were essentially higher than the levels of errors in simulated coatings. Average errors, obtained in the course of CME, do not exceed 4%–5%, and errors estimated from the real experimental data reach 10%–11% for some layers. In addition to this, patterns of errors shown in Figs. 4 and 2 are rather different. Along with the differences between DF_{sim} and DF_{exp} values, this indicates that there was no adequate correspondence between simulated and real deposition processes.

Inconsistency between levels of simulated errors and estimated real errors, as well as reproducibility of estimated real errors from one deposition run to another, indicates that the simulation, deposition, and probably reverse engineering processes were not properly correlated in our design–production chain (see the right-hand part of Fig. 1). In order to adequately interconnect the elements of the chain, we considered several suppositions that may explain the obtained inconsistencies:

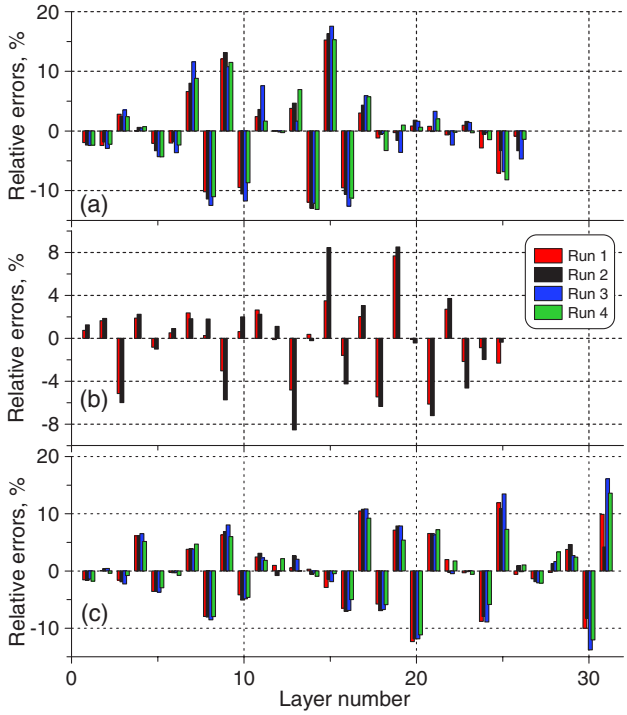

Fig. 4. (Color online) Relative errors in layer thicknesses of produced coatings: (a) NBPF1, (b) NBPF2, and (c) TLF1 estimated on the basis of minimization of the generalized discrepancy function [Eq. (4)].

Supposition A. There are systematic factors caused by deficiencies of the coating model itself (for example, inhomogeneity, scattering, effects of thin intermediate layers were not taken into account by the used model) or errors in the specified parameter data set (for example, errors in optical constants of layers). If such factors were not taken into account by the BBM procedure in the course of the deposition, then the BBM could not control the deposition process in an optimal way.

Supposition B. There were essential factors that were not taken into account in the course of the CME. It means that there was no correspondence between simulated and real deposition processes in our design–production chain.

Supposition C. The reverse engineering model, which was applied for experimental data processing, was missing significant factors and therefore was not sufficient. It means that there was no proper relationship between deposition and reverse engineering in the design–production chain.

Our primary goal was to check our suppositions and to make necessary corrections in our design–production chain. Realization of this goal allows us to improve the quality of the coatings and to open a way for performing reliable adequate CME.

3. Correlation between Simulation and Real Deposition Parameters

All major factors affecting the deposition process and causing errors in layer parameters can be divided into two groups. The factors of the first group are related to the deposition process and monitoring system. It includes, for example, random noise in experimental transmittance data, measurement fluctuations, shutter delays, and deposition rates and their fluctuations. In order to minimize systematic errors, careful calibration of the system was performed. The shutters were calibrated to reduce fluctuations during closing. The mean shutter delay in the adjustment used was measured as 350 ms, and the fluctuations were in the range of 80 ms. In the case of the LZH simulator, in order to quantify the existing errors in the measurement system, a large number of transmittance measurements of well known substrates were made. A statistical evaluation of these measurements provided the information about random noise and measurement fluctuations. Measurement fluctuations of the whole transmittance curve were estimated as 0.15%, and the spectral distribution of noise was found from these measurements; the average level of noise is 1%. In the case of the OptiLayer simulator, measurement fluctuations of the whole transmittance curve were taken equal to 0.15%, the noise level was taken equal to 1%. This noise level was independent of the wavelength.

Deposition rates of the given system are 0.3 nm/s for TiO_2 and 0.56 nm/s for SiO_2. These rates are also used in the CME with fluctuations of to 3% for TiO_2 and 12% for SiO_2. Generally, the factors of the first group were adequately specified in the course of the CME.

The factors of the second group are related to the optical coating model. This model is defined by the refractive indices and extinction coefficients of the layer materials and the substrate, presence of bulk inhomogeneity, surface roughness, thickness dependence of the refractive indices, etc. [29]. Evidently, it is not realistic to include all factors accurately in the coating model. For this reason, the optical coating model, used by BBM to control the deposition, should take into account the most important features of the process, but this model should remain simple enough. In our research we considered variations in the optical constants of the layers as the most probable factors causing errors in the course of deposition.

In the case of the Leybold SYRUSpro1100 deposition plant, the nominal optical constants were determined on the basis of *ex situ* single layer and multilayer characterization. It is known that the optical constants of films in multilayer stacks can be slightly different from the refractive indices of single layers [30,31]. It is also possible that the refractive indices of films of different thicknesses have different dispersion behavior, as is shown in [32,33]. This phenomenon is attributed to different crystalline fractions in films of different thicknesses. From both physical and technological points of view, deposition of optical coatings is a complicated process, and variations in the dispersion behavior of refractive indices can be caused by various factors inside the deposition plant: change of material in the melting pot during the deposition, unstable ion assisting because of the temperature and cathode lifetime of the APSpro source, variations in deposition rates with changes in the melting pot filling or conditions of the melt (crystals in the case of SiO_2), unstable temperature conditions of the substrate at the start of the deposition, cleaning conditions of the coating plant, etc.

We studied the influence of refractive index variations on the deposition process with the use of *trial* CME. In the course of these experiments we specified the same levels of errors in measurement data and the same estimations of rates as for starting CME described in Section 2. For refractive indices, we tried various combinations of errors, namely, offsets of refractive index dispersion curves, index drifts, and offsets of Sellmeier coefficients. For the extinction coefficient we specified offsets. We tried various reasonable variations of optical constants, namely the following:

- We specified offsets Δn_H and Δn_L of the high and low refractive indices and substituted $n_H(\lambda) + \Delta n_H$ and $n_L(\lambda) + \Delta n_L$ into Eq. (1) instead of the nominal refractive indices $n_H(\lambda)$ and $n_L(\lambda)$. Offset values were varied in the range from 0.3% to 2% for TiO_2 and from 0.5% to 1% for SiO_2.
- We supposed that the TiO_2 refractive index is dependent on TiO_2 film thickness z and specified linear drift for high-index layers. We substituted $n_H(\lambda; z) = n_H(\lambda)(1 - \delta(z[\text{nm}]/100[\text{nm}]))$ in Eq. (1) instead of the nominal TiO_2 refractive index. We took δ values up to -0.003.
- We varied the TiO_2 and SiO_2 dispersion curves. For this purpose we specified offsets of Sellmeier coefficients. For TiO_2, we substituted $A_1(1 + \Delta A_1)$, $A_2(1 + \Delta A_2)$ into Eq. (1) instead of A_1, A_2. We took ΔA_1 from the range [0.5%–1.5%] and ΔA_2 from the range [–5% to –10%]. For SiO_2 we varied ΔA_1 in the range [–4%; 4%] and ΔA_2 in the range [600%–700%]. It should be noted here that the large ΔA_2 resulted from small Selmeier coefficients.
- Instead of $k(\lambda)$ values we tried $\alpha k(\lambda)$ with α from 0.5 to 4.

We repeated CME with various sets of simulation parameters, trying to reproduce the situation observed in real deposition runs. Namely, we used trial and error methods and searched for parameters that provided simulated coatings satisfying the following conditions:

1. These coatings were to exhibit spectral transmittances $T(d_1, \ldots, d_k; \lambda)$ similar to the ones obtained in the course of real deposition runs. It means that the spectral behavior of deviations between theoretical and measurement transmittance curves should be similar.

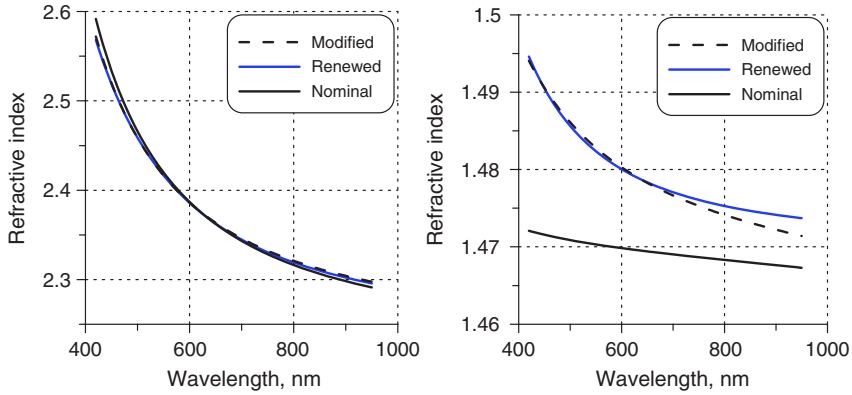

Fig. 5. (Color online) *Modified* refractive indices of TiO_2 and SiO_2, refractive indices determined by the *renewed* reverse engineering procedure from a typical simulated data set, and *nominal* TiO_2 and SiO_2 refractive indices.

2. The discrepancy function values calculated for simulated coatings DF_{sim} were to be close to the discrepancies obtained in the real deposition runs DF_{exp} listed in Table 3.

3. For different simulation runs, estimations of relative errors in layer thicknesses obtained on the basis of minimization of function [Eq. (4)] were to be reproduced from run to run. Moreover, the patterns of these errors were to be similar to those found from the experimental data (see Fig. 4).

As a result of numerous CME, we found the following corrected expressions for layer refractive indices:

$$n^2(\lambda) = 1 + \frac{A_1(1+\Delta A_1)\lambda^2}{\lambda^2 - A_2(1+\Delta A_2)} + \frac{A_3\lambda^2}{\lambda^2 - A_4}, \qquad (5)$$

where $\Delta A_1 = 1.1\%$, $\Delta A_2 = -7\%$ for TiO_2 and $\Delta A_1 = -3.5\%$, $\Delta A_2 = 700\%$ for SiO_2. Extinction coefficient values were taken three times higher than nominal values presented in Section 2. We shall refer to optical constants obtained in this way as to *modified optical constants*. Nominal and modified refractive indices of TiO_2 and SiO_2 are presented in Fig. 5, and nominal and modified extinction coefficients of TiO_2 are shown in Fig. 6.

We performed a number of CME assuming that the considered optical coatings were described by a model with modified optical constants but the BBM procedure did not take them into account and used nominal refractive indices. In other words, simulated transmittance data were calculated for coatings with modified optical constants, and the BBM procedure controlled layer thicknesses assuming that the optical constants were nominal ones. We call these CME as *renewed CME*.

Typical relative errors in layer thicknesses, obtained in the course of renewed CME for the NBPF1 design are shown in Fig. 7. The average discrepancy DF_{sim} obtained in the course of 50 CME is 5.2. This value is very close to the discrepancies DF_{exp} achieved in the course of real deposition runs (see the second column of Table 3).

We performed a reverse engineering procedure for the simulated coatings obtained in the course of the renewed CME. We estimated relative errors in layers thicknesses only, i.e., our process was based on the minimization of function [Eq. (4)]. Typical estimations of relative errors in the NBPF1 design are shown in Fig. 8. In this figure we also present estimations of the errors in layer thicknesses obtained from the experimental data related to deposition Run1 of NBPF1. It is seen that the levels of errors and pattern of errors, estimated from simulated data and from experimental data, are quite close.

This similarity, closeness between discrepancies DF_{sim} and DF_{exp}, and similarity in spectral transmittance data measured after the deposition of each layer indicate that with the help of simulations we managed to reproduce the situation observed in the real deposition experiments with sufficient reliability.

Based on the analysis of the CME results, we found a systematic factor strongly affecting the monitoring procedure and, as a consequence, the whole deposition process. It turned out that the BBM monitoring procedure used inconsistent refractive indices of the TiO_2 and SiO_2 layers as well as underestimating the extinction coefficient of the TiO_2 layers. In other

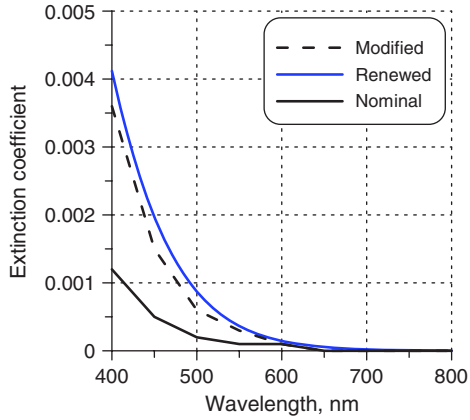

Fig. 6. (Color online) *Modified* extinction coefficient of TiO_2, extinction coefficient of TiO_2 determined by the *renewed* reverse engineering procedure, and *nominal* TiO_2 extinction coefficient.

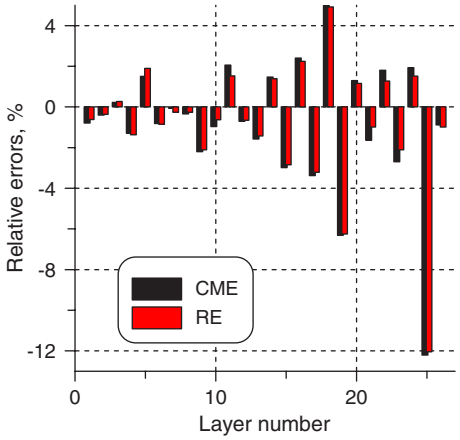

Fig. 7. (Color online) Comparison of relative errors in layer thicknesses of NBPF1: typical errors obtained in the course of *renewed CME* and errors determined by the *renewed reverse engineering* procedure.

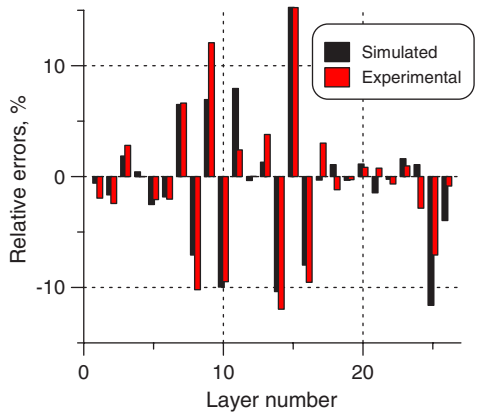

Fig. 8. (Color online) Relative errors in layer thicknesses estimated by the reverse engineering procedure from a typical *simulated* data set and errors determined by the reverse engineering procedure from the *experimental* data set related to NBPF1 Run 1. Reverse engineering procedure was based on minimization of the generalized discrepancy function [Eq. (4)]

words, the BBM algorithm tried to handle errors in layer thicknesses using an inconsistent model of a multilayer coating. It means that Supposition A, mentioned above, was true. In order to reduce the influence of this systematic factor and improve the quality of the deposited coatings, our monitoring procedure should use variations of the refractive indices and extinction coefficients. In the next section we demonstrate new experimental samples with improved spectral performance.

At the same time, renewed CME convinced us that Supposition B was true, and we found a factor that was not taken into account in the course of CME. It means that in the next CME we shall have to take into account modified refractive index and extinction coefficient wavelength dependencies.

4. Validation of the Reverse Engineering Procedure

In order to finish setting up proper relations between the elements of our design–production chain, we verified Supposition C. In the previous section we found that the optical coating parameter set used in the course of BBM was inconsistent. In turn, the reverse engineering procedure was also inconsistent, because it was based on a wrong supposition about the reliability of optical constants. Therefore, the optical coating parameter set used in the reverse engineering procedure must take into account possible variations of dispersion curves. We proposed to specify a more realistic coating model and searched for not only random errors in layer thicknesses but also variations of optical constant wavelength dependencies. Our *renewed* reverse engineering procedure is based on the minimization of the modified discrepancy function (*MDF*):

$$MDF = \left(\frac{1}{NL} \sum_{k=1}^{N} \sum_{j=1}^{L} [T(d_1(1+\delta_1), \ldots, d_k(1+\delta_k); p_1, p_2, q; \lambda_j) - \hat{T}^{(k)}(\lambda_j)]^2 \right)^{1/2}, \quad (6)$$

where $p_{1,2} = \{A, B, C\}$ specify a Cauchy model for the refractive indices of TiO_2 and SiO_2: $n(\lambda) = A + B(1000/\lambda)^2 + C(1000/\lambda)^4$; $q = \{B_0, B_1, B_2\}$ describes an exponential model for the TiO_2 extinction coefficient: $k(\lambda) = B_0 \exp\{B1 \cdot (1000/\lambda) + B2 \cdot (\lambda/1000)\}$. We used a Cauchy model because it has less parameters than a Sellmeier one and provides quite similar spectral dependence of refractive indices in the limited spectral range from 420 to 950 nm.

First, we applied the renewed reverse engineering procedure to the simulated data sets. In Fig. 7 we compared errors in layer thicknesses, determined in the course of the renewed reverse engineering process, and errors obtained in the course of the BBM simulations. In Figs. 5 and 6 we compared the modified optical constants of TiO_2 and SiO_2 and the dependencies, determined in the course of the renewed reverse engineering procedure. In Figs. 5, 6, and 7 one can observe good agreement between the results. This agreement validates our renewed reverse engineering procedure.

We applied the renewed reverse engineering procedure to the experimental data sets related to the produced samples of NBPF1, NBPF2, and TLF1 and found the model parameters of these coatings. In all cases, obtained TiO_2 and SiO_2 refractive indices were close to those used in the renewed CME. The errors in layer thicknesses found for the NBPF1 runs are presented in Fig. 9. The refractive indices of the TiO_2 and SiO_2 layers determined by the renewed reverse engineering procedure are presented in Fig. 10. In this figure one can observe that dispersion curves of SiO_2 are only shifted with respect to the modified refractive index of SiO_2, and the pattern of this dispersion is not changed.

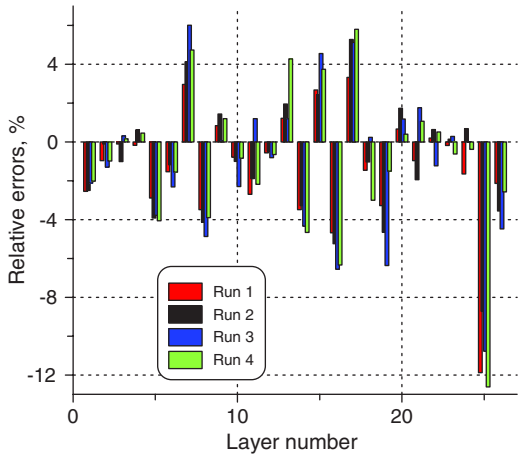

Fig. 9. (Color online) Relative errors in layer thicknesses of produced NBPF1 coatings determined by the renewed reverse engineering procedure.

Estimations of the TiO_2 extinction coefficient were approximately 2.5–3.5 times higher than their nominal values. The achieved values of the modified discrepancy function [Eq. (6)] were approximately two times lower than discrepancy function values achieved in the course of the reverse engineering procedure based on Eq. (4). These values are compared in Table 4.

5. Feedback to the Deposition Process

In order to verify the reliability of our conclusions, we produced new experimental samples of the NBPF1 and NBPF2 designs. In the theoretical designs we replaced the nominal optical constants of the layer materials by the modified optical constants. This also required a refinement of the thicknesses of the theoretical designs. In the case of the NBPF1 design, we refined the thicknesses of only the last two layers. Geometrical thicknesses of the 25th and 26th layers became 13.8 and 122.73 nm, respectively. In the case of the NBPF2 design, we refined all layer thicknesses, allowing thickness variations in the range of 1%. For this purpose we used a constrained optimization algorithm incorporated in the OptiLayer software [9,34]. As a result, the refined designs have the same theoretical spectral characteristics as the initial designs described in Table 1.

In Fig. 11 we present transmittance data of the three new experimental NBPF1 samples and transmittance data of the two new NBPF2 samples. We also present theoretical transmittance data of the NBPF1 and NBPF2 designs calculated with the modified optical constants. In Tables 5 and 6 we compare discrepancies DF_{exp} and $DF_{\mathrm{exp}}^{(t)}$ calculated from the experimental data related to the first series of deposition runs of NBPF1 and NBPF2 with the

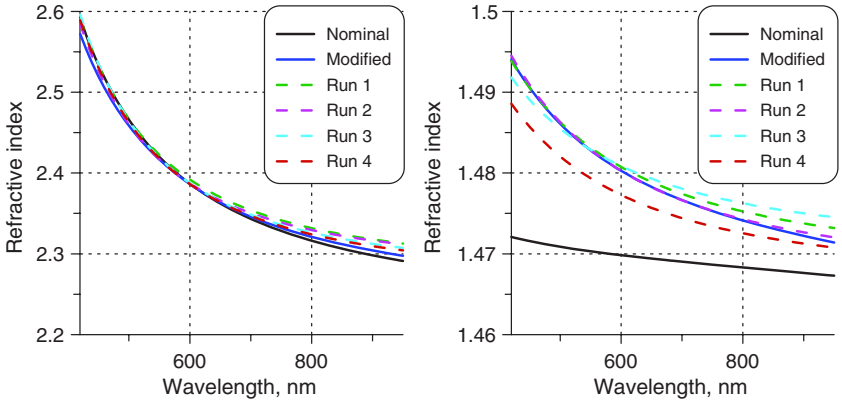

Fig. 10. (Color online) Dashed curves indicate refractive indices of TiO_2 (left side) and SiO_2 (right side) determined by the renewed reverse engineering procedure from experimental data related to produced NBPF1 coatings (Runs 1–4). Black curves show nominal refractive index values, and blue curves present modified refractive index values.

Table 4. Comparison of Generalized Discrepancy Function Values Calculated for Experimental Samples

Design (Run)	*GDF* Calculated from Measured Data	*GDF* Achieved by Rev. Eng. Procedure based on Eq. (4)	*GDF* Achieved by Rev. Eng. Procedure based on Eq. (6)
NBPF1 (1)	3.0	1.1	0.5
NBPF1 (2)	3.5	1.0	0.5
NBPF1 (3)	3.8	1.1	0.5
NBPF1 (4)	3.4	1.1	0.5
NBPF2 (1)	2.2	1.3	0.5
NBPF2 (2)	2.4	1.4	0.6
TLF1 (1)	2.95	1.0	0.6
TLF1 (2)	2.9	1.0	0.8
TLF1 (3)	2.9	1.0	0.6
TLF1 (4)	3.1	1.0	0.6

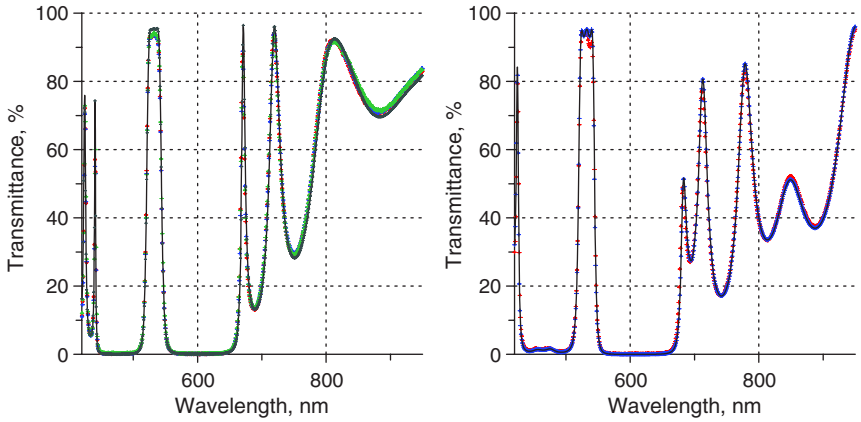

Fig. 11. (Color online) Solid curves present theoretical transmittances of the designs NBPF1 (left side) and NBPF2 (right side). Crosses show the experimental transmittance data corresponding to the deposition runs with the new dispersion data.

Table 5. Comparison of Discrepancies Calculated for NBPF1 Experimental Samples

Deposition Run	DF_{exp}	$DF^{(t)}_{exp}$	*GDF*
Run1	5.4	1.1	2.9
Run2	6.4	1.7	3.5
Run3	6.7	2.7	3.6
Run4	5.8	1.5	3.1
Run5	**3.0**	**0.9**	**1.7**
Run6	**2.9**	**1.0**	**1.6**
Run7	**3.2**	**0.9**	**1.7**

Table 6. Comparison of Discrepancies Calculated for NBPF2 Experimental Samples

Deposition Run	DF_{exp}	$DF^{(t)}_{exp}$	*GDF*
Run1	4.0	2.2	2.2
Run2	4.8	2.9	2.4
Run3	**1.9**	**1.4**	**1.2**
Run4	**2.1**	**1.4**	**1.3**

nominal optical constants and to the new series of deposition runs with the modified optical constants. In these tables we also compare the values of the generalized discrepancy function *GDF* calculated for the first deposition runs and the new deposition runs of the NBPF1 and NBPF2 designs. It is seen from Tables 5 and 6 that all DF_{exp}, $DF^{(t)}_{exp}$, and *GDF* values calculated for the new NBPF1 and NBPF2 samples are significantly lower than these values corresponding to the first NBPF1 and NBPF2 samples.

We provided feedback to the deposition process and demonstrated on the basis of the experimental data that our conclusion about incorrect dispersion of the TiO_2 and SiO_2 optical constants, made on the basis of the CME, was true. We took into account the modified indices in the course of the deposition and significantly improved the performance of the deposited coatings.

6. Conclusions

In our study we demonstrated the benefits of using CME in modern design–production chains. Generally, we proposed an approach that allows researchers to reveal factors causing production errors. Computational simulation of real deposition runs is a key element in this approach. In order to find factors significantly affecting the deposition process, we proposed performing the following steps.

- It is recommended that a series of starting CME are performed and production yields of the considered design(s) are estimated. Then several experimental coatings are to be deposited.
- Errors in layer parameters are to be estimated using a reasonable reverse engineering procedure. The determined layer parameters and the parameters typically obtained in the course of CME have to be compared. If the levels and patterns of these parameters are essentially different (i.e., different patterns and levels of errors in layer thicknesses, different dispersion behavior of the refractive indices, overestimations or underestimations of extinction coefficients), this is to be considered an indication of inconsistency between the simulation and real deposition parameters.
- Trial CME should be performed in order to find factors in the deposition process (level of errors in the measurement data, estimations of deposition rates and their fluctuations) or in the optical coating model (variations of optical constants, absence of inhomogeneity or roughness, etc.) that were taken into account neither in CME nor in real experiments, nor by the chosen reverse engineering procedure. Accurate numerical values describing these factors should be estimated. In the course of trial CME, it is assumed that the considered factors are physically sensible.
- A number of CME with new factors and parameters should be performed in order to confirm that these found factors adequately model real situation in the deposition plant.
- The reverse engineering procedure should be validated using simulated measurement data.
- In order to provide feedback to the deposition, experiments with a modified coating model should be performed. If an essential decrease in discrepancies

between the theoretical and measured data is achieved, it can be considered an indication that the factors are found correctly.

The proposed approach allows one to establish proper relations between simulation, deposition, and reverse engineering processes. This approach can be used in any design–production chain equipped with an optical monitoring device, a simulation software tool, and reverse engineering algorithms.

This work was supported by the German Federal Ministry of Economics and Technology (research project TACo—Tailored Automated Coating, contract no. 16IN0407), the DFG Cluster of Excellence, Munich Centre for Advanced Photonics (http://www.munich-photonics.de), the Russian Fund of Basic Research (projects 10-07-00480-a and 11-07-91153a), and the Centre for Quantum Engineering and Space-Time Research (QUEST).

References

1. D. Ristau, H. Ehlers, S. Schlichting, and M. Lappschies, "State of the art in deterministic production of optical thin films," Proc. SPIE **7101**, 71010C (2008).
2. A. Tikhonravov, M. Trubetskov, and I. Kasahara, "Achievements and challenges in the design and production of high quality optical coatings," IEICE Trans. Electron. **E91-C**, 1622–1629 (2008).
3. H. Pulker, "Film deposition methods," in *Optical Interference Coatings*, N. Kaiser and H. K. Pulker, eds. (Springer-Verlag, 2003), pp. 131–153.
4. A. Zöller, M. Boos, H. Hagedorn, W. Klug, and C. Schmitt, "High accurate in-situ optical thickness monitoring for multilayer coatings," in *Society of Vacuum Coaters 47th Annual Technical Conference Proceedings* (Society of Vacuum Coaters, 2004), pp. 72–75.
5. B. Badoil, F. Lemarchand, M. Cathelinaud, and M. Lequime, "Interest of broadband optical monitoring for thin-film filter manufacturing," Appl. Opt. **46**, 4294–4303 (2007).
6. S. Wilbrandt, O. Stenzel, and N. Kaiser, "Experimental determination of the refractive index profile of rugate filters based on in situ measurements of transmission spectra," J. Phys. D **40**, 1435–1441 (2007).
7. H. Ehlers, S. Schlichting, and D. Ristau, "Hybrid process control for precision optics enhanced by computational manufacturing," in *Optical Interference Coatings*, 2011 OSA Technical Digest Series (Optical Society of America, 2011), paper TuC6.
8. D. Ristau, "Characterization and monitoring," in *Optical Interference Coatings*, N. Kaiser and H. K. Pulker, eds. (Springer-Verlag, 2003), pp. 181–205.
9. A. V. Tikhonravov and M. K. Trubetskov, OptiLayer Thin Film Software, http://www.optilayer.com.
10. A. V. Tikhonravov, M. K. Trubetskov, and G. W. DeBell, "Optical coating design approaches based on the needle optimization technique," Appl. Opt. **46**, 704–710 (2007).
11. O. Stenzel, S. Wilbrandt, D. Fasold, and N. Kaiser, "A hybrid in situ monitoring strategy for optical coating deposition: application to the preparation of chirped dielectric mirrors," J. Opt. A **10**, 085305 (2008).
12. S. Wilbrandt, O. Stenzel, and N. Kaiser, "All-oxide broadband antireflection coatings by plasma ion assisted deposition: design, simulation, manufacturing and re-optimization," Opt. Express **18**, 19732–19742 (2010).
13. T. Gross, M. Lappschies, K. Starke, and D. Ristau, "Systematic errors in broadband optical monitoring," in *Optical Interference Coatings*, 2001 OSA Technical Digest Series (Optical Society of America, 2001), paper ME4.
14. M. Lappschies, T. Gross, H. Ehlers, and D. Ristau, "Broadband optical monitoring for the deposition of complex coating designs," Proc. SPIE **5250**, 637–645 (2004).
15. K. Starke, T. Gross, M. Lappschies, and D. Ristau, "Rapid prototyping of optical thin film filters," Proc. SPIE **4094**, 83–92 (2000).
16. A. V. Tikhonravov and M. K. Trubetskov, "Computational manufacturing as a bridge between design and production," Appl. Opt. **44**, 6877–6884 (2005).
17. S. Schlichting, K. Heinrich, H. Ehlers, and D. Ristau, "Online re-optimization as a powerful part of enhanced strategies in optical broadband monitoring," Proc. SPIE **8168**, 81681E (2011).
18. A. V. Tikhonravov, M. K. Trubetskov, T. V. Amotchkina, and M. A. Kokarev, "Key role of the coating total optical thickness in solving design problems," Proc. SPIE **5250**, 312–321 (2004).
19. H. Ehlers, S. Schlichting, C. Schmitz, and D. Ristau, "Adaptive manufacturing of high-precision optics based on virtual deposition and hybrid process control techniques," Chin. Opt. Lett. **08**, 62–66 (2010).
20. A. V. Tikhonravov, M. K. Trubetskov, T. V. Amotchkina, and V. Pervak, "Estimations of production yields for choosing of a practically optimal optical coating design," Appl. Opt. **50**, C141–C147 (2011).
21. T. V. Amotchkina, M. K. Trubetskov, V. Pervak, and A. V. Tikhonravov, "Design, production and reverse engineering of two-octave antireflection coatings," Appl. Opt. **50**, 6468–6475 (2011).
22. M. Tilsch, K. Hendrix, and P. Verly, "Optical interference coating design contest 2004," Appl. Opt. **45**, 1544–1554 (2006).
23. A. Thelen, A. V. Tikhonravov, M. K. Trubetskov, M. Tilsch, and U. Brauneck, "Topical meeting on optical interference coatings (OIC '2001): design contest results," Appl. Opt. **41**, 3022–3038 (2002).
24. K. Friedrich, S. Wilbrandt, O. Stenzel, N. Kaiser, and K. Hoffmann, "Computational manufacturing of optical interference coatings: method, simulation results, and comparison with experiment," Appl. Opt. **49**, 3150–3162 (2010).
25. D. Ristau, H. Ehlers, T. Gross, and M. Lappschies, "Optical broadband monitoring of conventional and ion processes," Appl. Opt. **45**, 1495–1501 (2006).
26. T. V. Amotchkina, M. K. Trubetskov, V. Pervak, S. Schlichting, H. Ehlers, D. Ristau, and A. V. Tikhonravov, "Comparison of algorithms used for optical characterization of multilayer optical coatings," Appl. Opt. **50**, 3389–3395 (2011).
27. "Quartz glass for optics: data and properties," http://heraeus-quarzglas.com.
28. A. V. Tikhonravov and M. K. Trubetskov, "On-line characterization and reoptimization of optical coatings," Proc. SPIE **5250**, 406–413 (2004).
29. B. T. Sullivan and J. A. Dobrowolski, "Deposition error compensation for optical multilayer coatings. I. Theoretical description," Appl. Opt. **31**, 3821–3835 (1992).
30. A. V. Tikhonravov, T. V. Amotchkina, M. K. Trubetskov, R. Francis, V. Janicki, J. Sancho-Parramon, H. Zorc, and V. Pervak, "Optical characterization and reverse engineering based on multiangle spectroscopy," Appl. Opt. **51**, 245–254 (2012).
31. A. Tikhonravov, M. Trubetskov, T. Amotchkina, A. Tikhonravov, D. Ristau, and S. Günster, "Reliable determination of wavelength dependence of thin film refractive index," Proc. SPIE **5188**, 331–342 (2003).
32. M. Modreanu, J. Sancho-Parramon, D. O'Connell, J. Justice, O. Durand, and B. Servet, "Solid phase crystallisation of HfO_2 thin films," Mater. Sci. Eng. B **118**, 127–131 (2005).
33. M. Modreanu, J. Sancho-Parramon, O. Durand, B. Servet, M. Stchakovsky, C. Eypert, C. Naudin, A. Knowles, and F. Bridou, "Investigation of thermal annealing effects on microstructural and optical properties of HfO_2 thin films," Appl. Surf. Sci. **253**, 328–334 (2006).
34. T. V. Amotchkina, J. Sancho-Parramon, V. Janicki, M. K. Trubetskov, H. Zorc, and A. V. Tikhonravov, "Design of multilayer coatings containing metal island films," Proc. SPIE **8168**, 816809 (2011).